Duty-cycle plus phase-shift control for a dual active half bridge based bipolar DC microgrid

Fei Gao and Dan Rogers
Department of Engineering Science,
University of Oxford,
Oxford, United Kingdom

***Abstract*—This paper studies the dual active half bridge when used to achieve flexible (symmetric or asymmetric) bipolar DC output. The circuit is operated with combined duty-cycle and phase-shift control to provide voltage splitting functionality without the requirement for an additional voltage balancing circuit. This topology uses reduced number of components needed to achieve the flexible bidirectional DC bipolar output with galvanic isolation, and has potential applications in low-cost bipolar DC microgrids. Depending on the relationship of the duty cycle and phase shift ratio, six different working cases are analyzed and corresponding power transfer is derived. Using a laboratory prototype, the performance of this dual active half bridge converter was further validated by experimental tests.**

Keywords—Dual active half bridge; phase shift; duty cycle; Asymmetric operation

I. INTRODUCTION

DC microgrids (MGs) have so far attracted more attentions because of advantages such as reduced cable losses, increased efficiency and absence of reactive power compensation [1]-[4]. Nowadays, the rapid development of renewable energy storage, hybrid electric vehicles, uninterruptible power supply, and smart grids has driven the popularity of bi-directional DC-DC converters, which have been widely used in DC MGs and more electric transportations [5]. Due to the advantages such as galvanic isolation, zero-voltage-switching, high power density, high efficiency, the dual active bridge (DAB) has been selected as a promising candidate for bidirectional DC-DC power conversion [6]-[10]. In a DAB, gate drive delays, device voltage drop, unmatched device transition times can result in an unequal volt-seconds during a switching cycle and consequently a non-zero DC current may arise. Hence, closed-loop control is often required to prevent DC flux build up in the DAB.

Under some circumstances, flexible DC output may be required. For instance, if the total output voltage is 48 V, 12 V and 36 V can be the split output voltage level instead of ±24 V. A voltage balancing circuit is needed if the upper arm voltage and lower arm voltage are either balanced or unbalanced [11]-[14]. In the existing literature, two-level voltage balancing circuit [11], three level voltage balancing circuit [12], dual-buck voltage balancer [13], trans-Z-source balancer [14] are proposed.

The research was conducted under the RHYTHM project (EP/N034570/1) and funded by the UK Engineering and Physical Science Research Council (EPSRC).

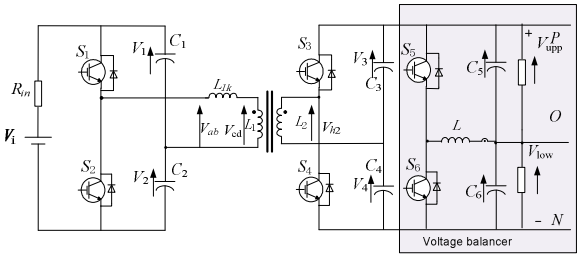

Fig. 1. A dual active half bridge with voltage balancing circuit.

Fig. 1 shows a DAHB with a voltage balancer at the right-hand side. The duty cycle of S_1-S_4 is 0.5 and the power transfer (or the output voltage) is regulated by the phase shift between the primary [S_1, S_2] and secondary bridge [S_3, S_4]. The DC output voltage across the upper and lower capacitors on the secondary side can be flexibly controlled by the additional switches by [S_5, S_6] respectively.

In contrast, the dual active half bridges (DAHB) topology (see Fig. 2) which uses less power devices and corresponding drive circuits is superior to the DAB in certain application scenarios, especially for lower power applications [15], [16]. With the combination of duty-cycle and phase-shift control, the upper-arm voltage and lower-arm voltage of the DAHB can be different. The DAHB which could have flexible bipolar output voltage without additional power conversion stages.

In the DAHB, he switches at the primary and/or secondary side can be controlled at non-0.5 duty-cycles. In this sense, the DAHB converter can behave as a two-port bipolar DC router with galvanic isolation, as shown in Fig. 3. Operation at a non-0.5 duty-cycle will lead to asymmetrical DC output for the corresponding side. If the duty-cycle at the primary side (D_p) is equal to the duty-cycle at secondary side (D_d), it is defined as *homogeneous operation* [17], [18]. On the other hand, if the primary-side duty cycle is different from secondary-side duty-cycle, it is defined as *heterogeneous operation*. Under heterogeneous operation, the DAHB could be used, for example, to connect a symmetric bipolar DC MG (primary-side duty-cycle is fixed at 0.5) to an asymmetric bipolar DC MG (secondary-side duty-cycle is non-0.5).

This paper focusses on the *heterogeneous* operation of a DAHB where the primary-side duty-cycle is fixed at 0.5 and the secondarys-side duty-cycle is non-0.5. Six possible working modes are analyzed and the corresponding

characteristic analysis are conducted. In addition, transformer RMS current is analyzed and compared with that under homogeneous operation.

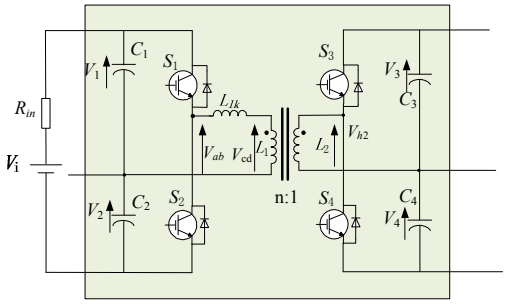

Fig. 2. A dual active half bridge.

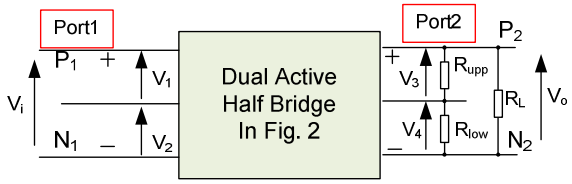

Fig. 3. Equivalent diagram of a two port DC microgrid.

II. Characteristic Analysis

A. Working Case

The duty-cycle on primary/secondary side will determine the voltage split ratio, as shown in the following equation:

$$V_1 = V_i(1-D_p),\ V_2 = V_i D_p,$$
$$V_3 = V_{upp} = V_o(1-D_d),\ V_4 = V_{low} = V_o D_d \quad (1)$$

where V_1, V_2 are the voltage across the capacitors C_1 and C_2; V_3 and V_4 are the voltage across the capacitors C_3 and C_4; V_i is the voltage at port 1; V_o is the voltage at port 2. Considering the general load condition of the bipolar output, R_{upp} and R_{low} represent the load on the upper and lower arm of the port 2 respectively. In addition, a load across the full output R_L is in presence.

This paper focuses on the case that the duty-cycle of the primary-side switches D_p is fixed to 0.5 whilst the duty-cycle of the secondary-side switches D_d varies. By ignoring the dead time effect of switches, depending on the relative positions of the switching signal of S_1 and S_3, there are six working cases, as listed in Table I. The voltage across the splitting capacitors C_1-C_4 can be expressed as follows:

$$V_1 = V_2 = \frac{V_{in}}{2},\ V_3 = V_{upp} = V_o(1-D_d),\ V_4 = V_{low} = V_o D_d \quad (2)$$

The potential six cases are illustrated in Fig. 4 and Fig. 5 shows the switching signals and key waveforms in these six cases. T_S is the switching period. Table II shows the relationship between duty-cycle and phase-shift in the listed six cases.

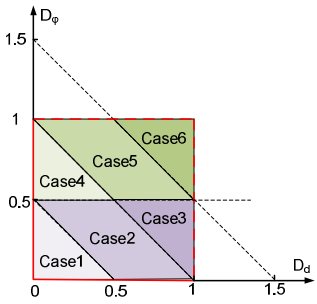

Fig. 4. Case location in the 2-D plane of phase-shift ratio and duty-cycle.

TABLE I. Different Cases

Cases	Relationship between D_φ and D_d
1	D_φ<0.5, $D_\varphi + D_d$<0.5, D_d <0.5
2	D_φ <0.5, 0.5 < $D_\varphi + D_d$ <1
3	D_φ <0.5, $D_\varphi + D_d$ >1
4	D_φ >0.5, $D_\varphi + D_d$ <1, D_d <0.5
5	D_φ >0.5, 1< $D_\varphi + D_d$ <1.5
6	D_φ >0.5, D_d >0.5, $D_\varphi + D_d$ >1.5

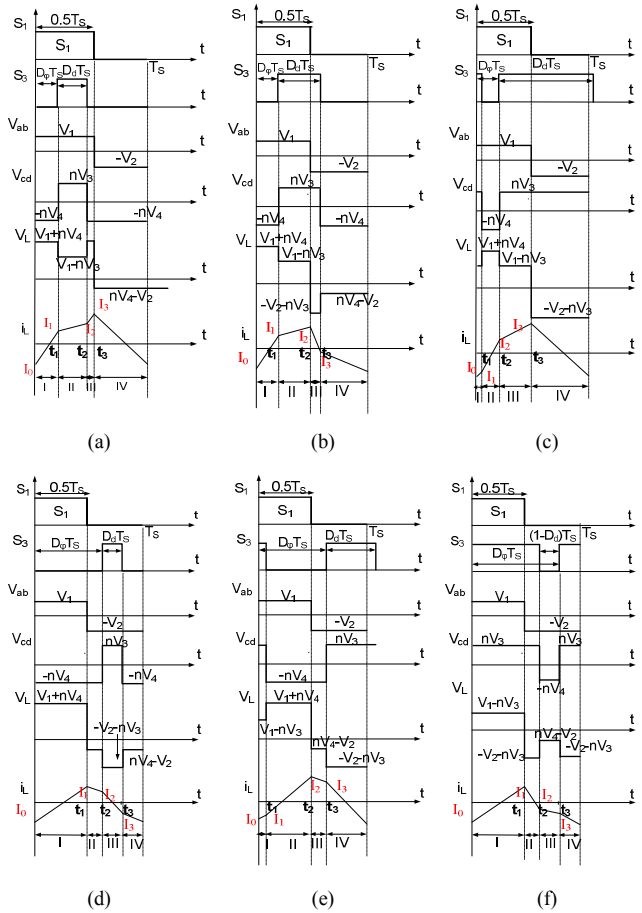

Fig. 5. Switching signals and key waveforms (a) case 1; (b) case 2; (c) case 3; (d) case 4; (e) case 5; (f) case 6.

B. Power Transfer

According to the case illustration shown in Fig. 5, the critical time point for six cases is listed in Table II and the corresponding voltage across the leakage inductor for six cases are shown in Table III.

TABLE II. CRITICAL POINT FOR DIFFERENT CASES

Case	t_1	t_2	t_3
1	$D_\varphi T_s$	$(D_\varphi+D_d)T_s$	$0.5T_s$
2	$D_\varphi T_s$	$0.5T_s$	$(D_\varphi+D_d)T_s$
3	$(D_\varphi-(1-D_d))T_s$	$D_\varphi T_s$	$0.5T_s$
4	$0.5T_s$	$D_\varphi T_s$	$(D_\varphi+D_d)T_s$
5	$(D_\varphi-(1-D_d))T_s$	$0.5T_s$	$D_\varphi T_s$
6	$0.5T_s$	$(D_\varphi-(1-D_d))T_s$	$D_\varphi T_s$

TABLE III. VOLTAGE ACROSS THE LEAKAGE INDUCTOR FOR SIX WORKING MODES

Case	V_L [0, t_1]	V_L [t_1, t_2]	V_L [t_2, t_3]	V_L [t_3, T_s]
1	V_1+nV_4	V_1-nV_3	V_1+nV_4	$-V_2+nV_4$
2	V_1+nV_4	V_1-nV_3	$-V_2-nV_3$	$-V_2+nV_4$
3	V_1-nV_3	V_1+nV_4	V_1-nV_3	$-V_2-nV_3$
4	V_1+nV_4	$-V_2+nV_4$	$-V_2-nV_3$	$-V_2+nV_4$
5	V_1-nV_3	V_1+nV_4	$-V_2+nV_4$	$-V_2-nV_3$
6	V_1-nV_3	$-V_2-nV_3$	$-V_2+nV_4$	$-V_2-nV_3$

It can be observed from Fig. 5 that there are four working stages (stage I-IV) in one cycle. The transformer current can be expressed as follows:

$$i_L(t)=\begin{cases}\dfrac{1}{L_{lk}}V_L t+I_0, & \text{Stage I}\\ \dfrac{1}{L_{lk}}V_L(t-t_1)+I_1, & \text{Stage II}\\ \dfrac{1}{L_{lk}}V_L(t-t_2)+I_2, & \text{Stage III}\\ \dfrac{1}{L_{lk}}V_L(t-t_3)+I_3, & \text{Stage IV}\end{cases} \tag{3}$$

As the average of the transformer current in one switching cycle is zero, the following equation is satisfied.

$$\int_0^{T_s} i_L dt=\int_0^{t_1} i_L dt+\int_{t_1}^{t_2} i_L dt+\int_{t_2}^{t_3} i_L dt+\int_{t_3}^{T_s} i_L dt=0 \tag{4}$$

The current values at the critical point (t_0-t_3) are marked as I_0-I_3, respectively. Thus, I_0-I_3 can be expressed as

$$\begin{cases}I_1=\dfrac{1}{L_{lk}}V_L t_1+I_0,\\ I_2=\dfrac{1}{L_{lk}}V_L(t_2-t_1)+I_1,\\ I_3=\dfrac{1}{L_{lk}}V_L(t_3-t_2)+I_2,\\ I_0=\dfrac{1}{L_{lk}}V_L(T_s-t_3)+I_3,\end{cases} \tag{5}$$

I_0-I_3 can be derived for different cases as follows:

Case 1

$$\begin{cases}I_0=A\left(-0.5V_i+0.25V_i+D_d(1-D_d-2D_\varphi)nV_o\right)\\ I_1=A\left(0.25V_i+2D_\varphi V_i-0.5(1+2D_\varphi)V_i+(1-D_d)D_d nV_o\right)\\ I_2=A\left(0.25V_i+2D_d V_i+2D_\varphi V_i-0.5(1+2D_s+2D_\varphi)V_i-nD_d V_o+nD_d{}^2V_o\right)\\ I_3=-A\left(0.25V_i+D_d(1+D_d+2D_\varphi)nV_o-0.5(V_i+2D_d nV_o)\right)\end{cases} \tag{6}$$

Case 2

$$\begin{cases}I_0=A\left(-0.5V_i+0.25V_i+D_d(1-D_d-2D_\varphi)nV_o\right)\\ I_1=A\left(0.25V_i+2D_\varphi V_i-0.5(1+2D_\varphi)V_i+n(1-D_d)D_d V_o\right)\\ I_2=-A\left(0.25V_i-(1-D_d)(D_d+2D_\varphi)nV_o-0.5(V_i-2(1-D_d)nV_o)\right)\\ I_3=A\left(0.25V_i+D_p(1-2D_d-2D_\varphi)V_i-(1-D_d)D_d nV_o\right)\end{cases} \tag{7}$$

Case 3

$$\begin{cases}I_0=A\left(-0.5V_i+0.25V_i-(1-D_d)(2-D_d-2D_\varphi)nV_o\right)\\ I_1=A\left(-0.5(0.5+2(1-D_d-D_\varphi))V_i-(1-D_d)D_d nV_o\right)\\ I_2=A\left(0.25V_i+2D_\varphi V_i-0.5(1+2D_\varphi)V_i+(1-D_d)D_d nV_o\right)\\ I_3=-A\left(0.25V_i-(1-D_d)(D_d+2D_\varphi)nV_o-0.5(V_i-2(1-D_d)nV_o)\right)\end{cases} \tag{8}$$

Case 4

$$\begin{cases}I_0=A\left(-0.5V_i+0.25V_i+D_d(1-D_d-2D_\varphi)nV_o\right)\\ I_1=-A\left(0.25V_i-D_d(1-D_d-2D_\varphi)nV_o-0.5(V_i+2D_d nV_o)\right)\\ I_2=A\left(0.25V_i+0.5(1-2D_\varphi)V_i+(1-D_d)D_d nV_o\right)\\ I_3=A\left(0.25V_i+0.5(1-2D_d-2D_\varphi)V_i-(1-D_d)D_d nV_o\right)\end{cases} \tag{9}$$

Case 5

$$\begin{cases}I_0=A\left(-0.5V_i+0.25V_i-(1-D_d)(2-D_d-2D_\varphi)nV_o\right)\\ I_1=A\left(-0.5(0.5+2(1-D_d-D_\varphi))V_i-(1-D_d)D_d nV_o\right)\\ I_2=-A\left(0.25V_i-D_d(1-D_d-2D_\varphi)nV_o-0.5(V_i+2D_d nV_o)\right)\\ I_3=A\left(0.25V_i+0.5(1-2D_\varphi)V_i+(1-D_d)D_d nV_o\right)\end{cases} \tag{10}$$

Case 6

$$\begin{cases}I_0=A\left(-0.5V_i+0.25V_i-(1-D_d)(2-D_d-2D_\varphi)nV_o\right)\\ I_1=-A\left(0.25V_i+(1-D_d)(2-D_d-2D_\varphi)nV_o-0.5(V_i-2(1-D_d)nV_o)\right)\\ I_2=A\left(0.25V_i+0.5(3-2D_d-2D_\varphi)V_i-(1-D_d)D_d nV_o\right)\\ I_3=A\left(0.25V_i+0.5(1-2D_\varphi)V_i+(1-D_d)D_d nV_o\right)\end{cases} \tag{11}$$

where A is

$$A=\frac{1}{2L_{lk}f_s} \tag{12}$$

The power transfer can be expressed as

$$P=\int_0^{T_s} V_L i_L dt=\int_0^{t_1} V_L i_L dt+\int_{t_1}^{t_2} V_L i_L dt+\int_{t_2}^{t_3} V_L i_L dt+\int_{t_3}^{T_s} V_L i_L dt \tag{13}$$

Combing the voltage across the leakage inductor (see Table III), (5), and (13), the power transfer expression can be written as follows:

$$P = \frac{KnV_{in}V_o}{8f_sL_{lk}} \tag{14}$$

where K depends on cases and can be derived as follows:

$$K = \begin{cases} D_d(-1+2D_d+4D_\varphi), & \text{case 1} \\ -(2D_d^2+(1-2D_\varphi)^2+D_d(-3+4D_\varphi)), & \text{case 2} \\ (-1+D_d)(-3+2D_d+4D_\varphi), & \text{case 3} \\ -D_d(-3+2D_d+4D_\varphi), & \text{case 4} \\ (2D_d{}^2+4(-1+D_\varphi)^2+D_d(-5+4D_\varphi)), & \text{case 5} \\ -(-1+D_d)(-5+2D_d+4D_\varphi), & \text{case 6} \end{cases} \tag{15}$$

It can be seen from (15) that the power transfer not only depends on the phase-shift ratio (D_φ) but also depends on the duty-cycle (D_d).

Fig. 6 shows the relationship between power transfer and duty-cycles with varying phase-shifts. It can be seen that the forward maximum power transfer occurs at case 2 when phase-shift ratio (D_φ) is 0.25 and duty-cycle (D_d) is 0.5 and reverse maximum power transfer occurs when phase-shift ratio (D_φ) is 0.75 and duty-cycle (D_d) is 0.5. The global maximum power transfer can be expressed as follows:

$$P_{\max} = \frac{nV_iV_o}{32f_sL_{lk}} \tag{16}$$

The power transfer direction depends on the relationship between phase-shift ratio and duty-cycle. It can be observed that given a fixed phase-shift ratio each power transfer curve is a piecewise function.

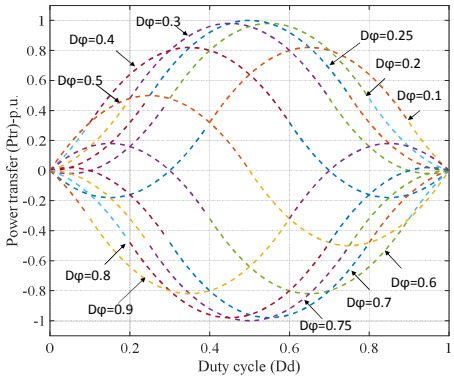

Fig. 6. Power transfer versus duty-cycle (D_d) under different phase-shift ratios (D_φ).

If the DAHB is loaded with R_{upp}, R_{low} and R_L, as shown in Fig. 3, the load power can be expressed as

$$P_o = \frac{V_o^2}{R_L} + \frac{V_3^2}{R_{upp}} + \frac{V_4^2}{R_{low}} \tag{17}$$

By substituting (2) into (17), one can obtain

$$P_o = V_o^2\left(\frac{1}{R_L} + \frac{(1-D_d)^2}{R_{upp}} + \frac{D_d{}^2}{R_{low}}\right) \tag{18}$$

Ignoring the transformer losses, the power transfer equals to the load power. By comparing (14), (15), and (18), the output voltage can be generally expressed as follows:

$$V_o = \frac{KnV_{in}}{8f_sL_{lk}\left(\frac{1}{R_L} + \frac{(1-D_d)^2}{R_{upp}} + \frac{D_d{}^2}{R_{low}}\right)} \tag{19}$$

It can be inferred from (19) that the output voltage is in proportional to the load resistance in an open loop condition. In other words, with the increase of the load resistance, the output voltage will increase.

III. Closed-Loop Control Scheme

This section will discuss the closed-loop control of the DAHB and compare the transformer RMS current under different operation scenarios.

A. Control Scheme

Closed-loop control schemes will be discussed in this subsection. As shown in Fig. 7. an outer loop controller can be added to tightly regulate the output voltage. The output of the voltage controller is the phase-shift ratio D_φ which should be limited between 0 and 1. An additional voltage controller is added to tune the duty-cycle. n_i stands for the ratio of the lower arm voltage to the full output voltage.

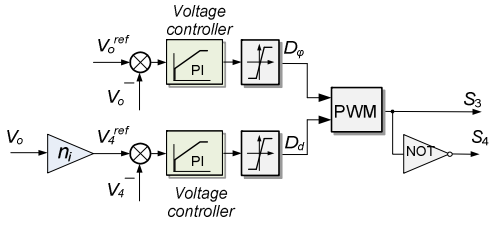

Fig. 7. Closed loop control scheme with duty cycle and phase shift control.

B. Comparison with Homogeneous Operation

As discussed in Section I, if the primary-side duty-cycle is set equal to the secondary-side duty-cycle D_d, it is defined as homogeneous operation. Is should naturally be expected that the transformer RMS current will be different under homogeneous and heterogeneous operation. Fig. 8 shows the comparison of the transformer RMS current in the heterogeneous operation (the subject of this paper) and homogeneous operation discussed in [15]. It can be seen that except for near-symmetrical output condition (i.e. near $D_p = D_d = 0.5$), homogeneous operation ($D_p = D_d$) results in a very significant reduction in the RMS current (and consequently a higher efficiency assuming similar component ratings). Therefore, homogenous operation would generally be preferred unless it is specifically required by the application that a symmetrical voltage split is maintained at the primary side.

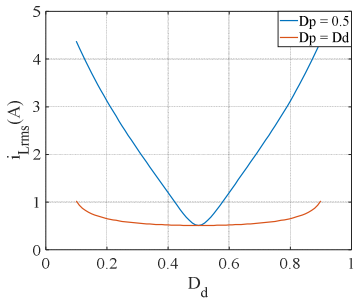

Fig. 8. Comparison of transformer RMS current of homogeneous and heterogeneous operation.

IV. Experimental Results and Discussion

The block diagram of the experimental setup is shown in Fig. 9. Port 1 of the DAHB is connected to 24 V whilst Port 2 is connected to a balanced load (R_{upp} = R_{low} = 10 Ω). Fig. 10 shows the lab prototype. Table IV lists the experimental parameters.

TABLE IV. Experimental Parameters

Description	Symbol	Value
Input voltage	V_{in}	24 V
Transformer ratio	n	1:1
Leakage inductor	L_{lk}	3 μH
Switching frequency	f_s	100 kHz
Splitting capacitor	C_1-C_4	1 mF

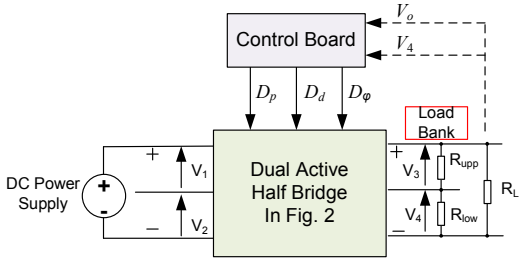

Fig. 9. Block diagram of experimental setup.

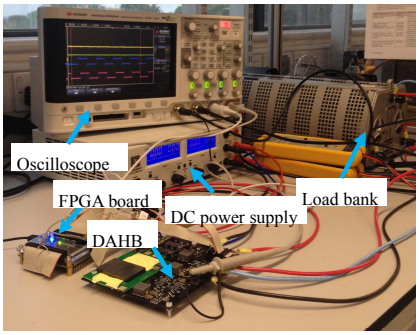

Fig. 10. Lab prototype.

A. Open-Loop Test

First, the open-loop tests have been conducted to demonstrate the potential working modes of the DAHB. Different combination of duty-cycles (D_d) and phase-shift D_φ are applied, as listed in Table V. Fig. 11(a)-(e) shows open loop tests for case 1-6 respectively. The output voltage agrees with (19) and steady state values of splitting voltages (V_2, V_4) are consistent with the expectation in (2).

TABLE V. Experimental Parameters

Period	Duty cycle	Phase shift	Case
(a)	0.2	0.1	1
(b)	0.4	0.15	2
(c)	0.8	0.3	3
(d)	0.2	0.6	4
(e)	0.9	0.9	6

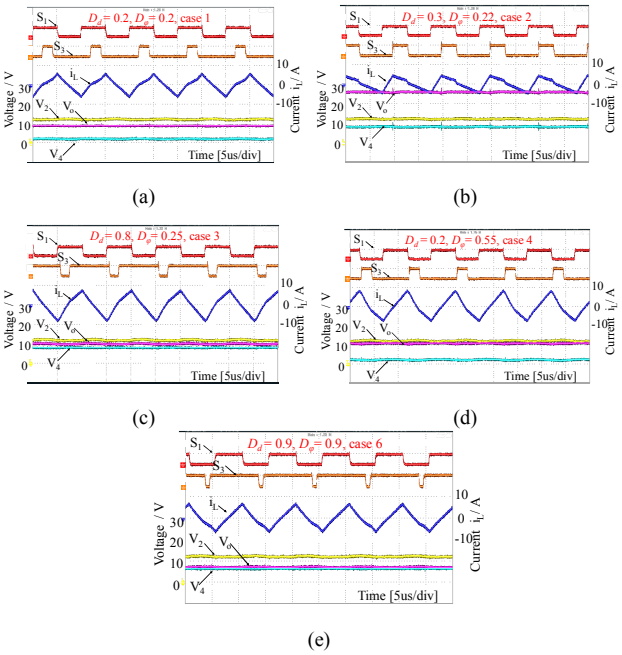

Fig. 11. Open loop test. (a) case 1; (b) case 2; (c) case 3; (d) case 4; (e) case 6.

B. Closed-Loop Test

In this test, a 35 Ω load R_L across the output port is applied. The feedback control scheme (see Fig. 7) is implemented. Output voltage reference V_o^{ref} is set at 24 V whilst the duty cycle varies, as listed in Table VI. The voltage split ratio n_i is set as 0.5, 0.2, 0.4, 0.7 respectively.

TABLE VI. Experimental Parameters

Period	Ratio (n_i)	Phase-shift calculation	Phase-shift measurement	error
(I)	0.5	0.056	0.06	7.1%
(II)	0.2	0.275	0.28	1.8%
(III)	0.4	0.113	0.12	6.2%
(IV)	0.7	0.983	0.98	0.3%

Fig. 12(a) shows the experimental result. It can be seen that the output voltage is tightly regulated at 24 V. The lower-arm primary-side voltage is fixed at 12 V whilst the lower-arm secondary-side voltage varies according to the set ratio n_i. Fig. 12(b)-(e) shows the zoomed steady state part in (I)-(IV) respectively. The phase-shift calculation from (19) is consistent with the observation in experimental test, which are listed in Table VI as well.

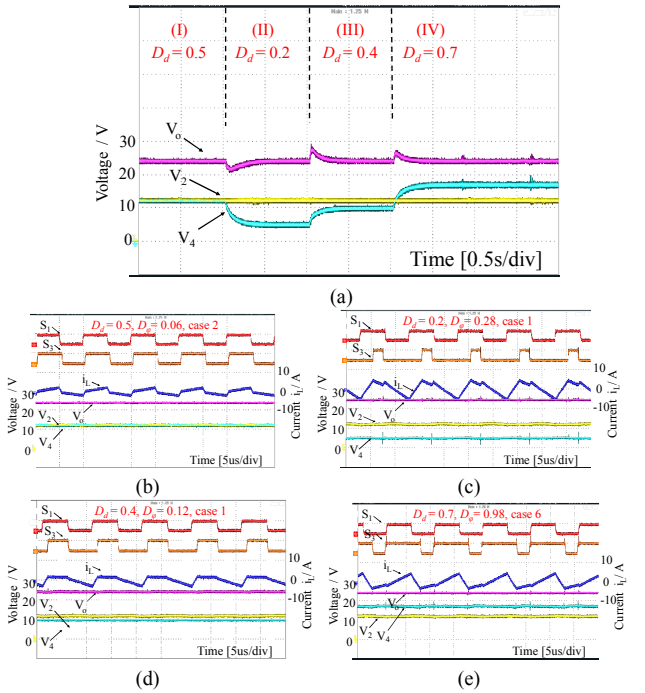

Fig. 12. Closed-loop experimental result. (a) Overview. (b) steady-state region in (I). (c) steady-state region in (II). (d) steady-state region in (III). (e) steady-state region in (IV).

C. *Homogeneous operation*

Fig. 13 shows the counterpart experimental result of Fig. 12 when the same secondary-side duty-cycle is also applied to the primary switch. By comparing Fig. 13(a)-(c) with Fig. 12(c)-(e), it can be clearly seen that the magnitude of the transformer current is reduced, indicating that the transformer RMS current is reduced under homogeneous operation. It supports the discussion in Section III.B.

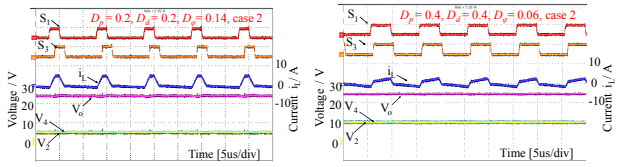

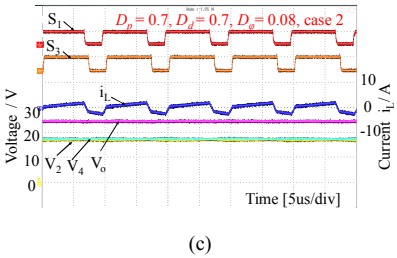

Fig. 13. Closed loop experimental result of homogenenous operation.

V. Conclusion

This paper has investigated the DAHB circuit operated with a fixed 0.5 primary-side duty-cycle and a variable secondary-side duty-cycle. Such a circuit may find applications in bipolar DC microgrids where it can achieve a flexible bipolar DC output with reduced number of components compared to a conventional DAB and voltage splitter circuit. Based on the relationship between the phase-shift and secondary-side duty-cycle, all possible working cases were analysed and corresponding power transfer functions were derived. A control scheme combining duty-cycle and phase-shift control was presented. Analysis of the transformer RMS current shows that it is preferable to operate the system in a homogeneous manner (equal primary and secondary-side duty cycles) in order to reduce the transformer losses, if this is possible in the application. The experimental results validate the behaviour of the DAHB under various working cases in open-loop and the good performance of the proposed closed-loop control scheme.

Acknowledgment

The authors are grateful to Mr. Efstratios Chatzinikolaou for his assistance in development of the hardware platform.

References

[1] H. J. Choi and J. H. Jung, "Enhanced power line communication strategy for DC microgrids using switching frequency modulation of power converters," *IEEE Trans. Power Electron.*, vol. 32, no. 6, pp. 4140–4144, Jun. 2017.

[2] F. Gao, et al, "Comparative stability analysis of droop control approaches in voltage source converters-based DC microgrids," *IEEE Trans. Power Electron.*, vol. 32, no. 3, pp. 2395–2415, Mar. 2017.

[3] L. Herrera, W. Zhang, and J. Wang, "Stability analysis and controller design of DC microgrids with constant power loads," *IEEE Trans. Smart Grid*, vol. 8, no. 2, pp. 881–888, Mar. 2017.

[4] F. Gao and S. Bozhko, "Modeling and impedance analysis of a single DC bus based multiple-source multiple-load electrical power system," *IEEE Trans. Transp. Electrif.* vol. 2, no. 3, pp. 335–346, Sep. 2016.

[5] B. Zhao, Q. Song, W. Liu, and Y. Sun, "Overview of dual-active-bridge isolated bidirectional DC–DC converter for high-frequency-link power-conversion system," *IEEE Trans. Power Electron.*, vol. 29, no. 8, pp. 4091–4106, Aug. 2014.

[6] X. Liu et al., "Novel dual-phase-shift control with bidirectional inner phase shifts for a dual-active-bridge converter having low surge current and stable power control," *IEEE Trans. Power Electron.*, vol. 32, no. 5, pp. 4095–4106, May 2017.

[7] G. G. Oggier, G. O. Garcia, and A. R. Oliva, "Modulation strategy to operate the dual active bridge DC-DC converter under soft switching in the whole operating range," *IEEE Trans. Power Electron.*, vol. 26, no. 4, pp. 1228–1236, Apr. 2011.

[8] B. Zhao, Q. Song, W. Liu, and Y. Sun, "A synthetic discrete design methodology of high-frequency isolated bidirectional DC/DC converter

for grid-connected battery energy storage system using advanced components," *IEEE Trans. Ind. Electron*., vol. 61, no. 10, pp. 5402–5410, Oct. 2014.

[9] F. Krismer and J. W. Kolar, "Closed form solution for minimum conduction loss modulation of DAB converters," *IEEE Trans. Power Electron*., vol. 27, no. 1, pp. 174–188, Jan. 2012.

[10] M. Pahlevaninezhad, P. Das, J. Drobnik, P. K. Jain, and A. Bakhshai, "A novel ZVZCS full-bridge DC/DC converter used for electric vehicles," *IEEE Trans. Power Electron*., vol. 27, no. 6, pp. 2752–2769, Jun. 2012.

[11] B-M. Han, "A half-bridge voltage balancer with new controller for bipolar DC distribution systems," *Energies*, vol. 9, no. 3, pp. 1–17, Mar. 2016.

[12] F. Wang, Z. Lei, X. Xu, and X. Shu, "Topology deduction and analysis of voltage balancers for DC micro-grid," *IEEE J. Emerg. Sel. Top. Power Electron.*, vol. 5, no. 2, pp.672–680, Jun. 2017.

[13] X. Zhang and C. Gong, "Dual-buck half-bridge voltage balancer," *IEEE Trans. Ind. Electron*., vol. 60, no. 8, pp. 3157–3164, Aug. 2013.

[14] S. Dadjo Tavakoli, J. Khajesalehi, M. Hamzeh, and K. Sheshyekani, "Decentralised voltage balancing in bipolar DC microgrids equipped with trans-z-source interlinking converter," *IET Renew. Power Gen.*, vol. 10, no. 5, pp. 703–712, May 2016.

[15] S. Chakraborty and S. Chattopadhyay, "Minimum-rms-current operation of asymmetric dual active half-bridge converters with and without ZVS," *IEEE Trans. Power Electron*., vol. 32, no. 7, pp. 5132–5145, Jul. 2017.

[16] P. He and A. Khaligh, "Comprehensive analyses and comparison of 1 kW isolated DC–DC converters for bidirectional EV charging systems," *IEEE Trans. Transp. Electrif*., vol. 3, no. 1, pp. 147–156, Mar. 2017.

[17] W. Jiang, L. Kai, R. Hu, and W. Chen, "Novel modeling and design of a dual half bridge DC-DC converter applied in supercapacitor energy storage system," *Electric Power Components and Systems*, vol. 42, no. 13, pp. 1398–1408, Sep. 2014.

[18] M. S. Irfan, A. Ahmed, J. H. Park, and C. Seo, "Current-sensorless power-decoupling phase-shift dual-half-bridge converter for DC–AC power conversion systems without electrolytic capacitor," *IEEE Trans. Power Electron*., vol. 32, no. 5, pp. 3610–3622, May 2017.